Eur. Phys. J. C manuscript No.
(will be inserted by the editor)

An Experiment for Electron-Hadron Scattering at the LHC

N. Armesto[a,1], **E. G. Ferreiro**[b,1], **M. Kumar** [h,10], **B. Mellado** [i,10,11], **J. G. Milhano**[c,2,5], **Y. Yamazaki**[d,4], **B. J. Holzer**[5], **K. D. J. André** [5,7], **O. S. Brüning**[5], **S.A. Bogacz**[6], **A. Polini**[e,8], **F. Kocak**[f,9], **P. Kostka**[g,7], **X. Ruan** [j,10]

[1]Instituto Galego de Física de Altas Enerxías IGFAE, Universidade de Santiago de Compostela, 15782 Santiago de Compostela, Galicia-Spain
[2]LIP, Av. Prof. Gama Pinto, 2, P-1649-003 Lisboa , Portugal
[3]Instituto Superior Técnico (IST), Universidade de Lisboa, Av. Rovisco Pais 1, 1049-001, Lisboa, Portugal
[4]Graduate School of Science, Kobe University, Rokkodai-cho 1-1, Nada, 657-8501 Kobe, Japan
[5]CERN, Esplanade des particules 1, 1211 Geneva 23, CH
[6]JLab, Newport News, Virginia, USA
[7]Liverpool University, Liverpool, L69 3BX, UK
[8]Istituto Nazionale di Fisica Nucleare (INFN), Sezione di Bologna, Bologna, Italy
[9]Bursa Uludag University, Bursa, Turkey
[10]School of Physics and Centre for Astrophysics, University of the Witwatersrand, Johannesburg, Wits 2050, South Africa.
[11]iThemba LABS, National Research Foundation, PO Box 722, Somerset West 7129, South Africa.

Received: date / Accepted: date

Abstract Progressive considerations are presented on the physics, apparatus and accelerator designs for a future, energy frontier electron-hadron scattering experiment at the LHC in the thirties. Owing to an energy recovery linac of 50 GeV electron beam energy, the LHeC achieves a centre of mass energy in *ep* scattering of 1.2 TeV, at an instantaneous luminosity of order $10^{34}\,\mathrm{cm}^{-2}\mathrm{s}^{-1}$. The apparatus and accelerator are designed to operate *ep* concurrently with the HL-LHC. A new default detector configuration is introduced, and the demands derived from physics are sketched. This detector is foreseen to be installed at IP2 for which for this time another detector is under study. Considerations on the detector design and the configuration of the interaction region are presented which entail the possibility to combine both tentative designs into one common experiment should that become of interest.

Keywords LHeC · Deep Inelastic Scattering · Higgs Boson · Energy Recovery Linac · Collider Detector · Interaction Region

[a]e-mail: nestor.armesto@usc.es
[b]e-mail: elena.gonzalez.ferreiro@usc.es
[c]e-mail: gmilhano@lip.pt
[d]e-mail: yamazaki@phys.sci.kobe-u.ac.jp
[e]e-mail: alessandro.polini@bo.infn.it
[f]e-mail: fkocak@uludag.edu.tr
[g]e-mail: peter.kostka@liv.ac.uk
[h]e-mail: Mukesh.Kumar@cern.ch
[i]e-mail: bmellado@mail.cern.ch
[j]e-mail: Xifeng.Ruan@cern.ch

1 Introduction

The Standard Model (SM) of particle physics is based on a non-Abelian gauge theory with a symmetry group $\mathrm{SU}(2)_L\times\mathrm{U}(1)\times\mathrm{SU}_c(3)$. The SM has and continues to enjoy great success in describing a wide span of phenomena emerging from interactions of particles at a range of energies that is accessible experimentally. That said, the SM is not a satisfactory theory of fundamental interactions nor does it explain a number of phenomena in nature. It is of paramount importance to the field of particle physics to establish how the SM breaks down in laboratory conditions. This is expected to be achieved by pushing the boundaries of energy and precision frontiers, and various sensitive experiments at low energy. Theory currently is less predictive than ever after the birth of the SM such that experimentation based on novel designs acquires a particular eminence for the decades ahead.

Deep inelastic scattering (DIS) of electrons off high energy protons (and ions) with high instantaneous luminosity offers a unique opportunity to enhance the precision frontier in particle physics, for which examples are provided in this paper. The intense, unique hadron beams of the LHC represent a salient opportunity to create a new laboratory for energy frontier DIS, the Large Hadron electron Collider (LHeC), at affordable cost: a larger than TeV CMS energy new collider is in sight by adding an energy recovery linac to the LHC, in possibly staged phases. The present paper is mainly devoted to an update of the detector, describing relevant physics, apparatus and accelerator design considerations and new results. The LHeC would be the fifth large collider experiment at the LHC facility, sustaining its future and exploiting the biggest investment in particle physics.

A first comprehensive design concept for the LHeC was published in 2012 [1], just weeks prior to the Higgs boson discovery and incorporating the findings of a review pursued by twenty experts in experimental, theoretical and accelerator physics. Following nearly ten years of LHC operation and analysis, incorporating technology progress, accounting for the advent of experimental Higgs physics and relying on the brilliant LHC performance, a further detailed report appeared recently, written again by representatives of more than a hundred institutions [3]. This paper presented the energy recovery, linac ring electron-hadron collider configuration as the selected default with luminosity parameters an order of magnitude enhanced compared to before. It suggested to downscope the electron beam energy from originally 60 to 50 GeV in an attempt to economise investments and efforts as the racetrack electron accelerator circumference then became comparable to that of the SPS.

The LHeC development followed the view that with the long shutdown (LS) 4, in the early thirties, the operation of the LHC as a heavy-ion collider would be terminated in order to maximise pp luminosity, which would free the Interaction Point (IP) 2 for a new experiment when the data taking for ALICE ended. Meanwhile one yet considers operating LHC with heavy ions further hence, while new considerations have appeared for a much smaller heavy-ion experiment configured to study soft heavy-ion interactions [4], while heavy-ion physics is newly discussed at LHCb too. The LHeC has been maintained as an option and complement of HL-LHC in strategic consideration of the future. Its programme naturally is that of complementing the TeV scale exploration with the LHC and a possible future e^+e^- collider, much like HERA was coupled to the Tevatron and LEP before.

As to IP2, in order to avoid a possible clash of the LHeC plan and that detector, sometimes termed “A3”, it had been suggested to evaluate whether the LHeC detector and the interaction region (IR) could be reconfigured to register and permit both ep/eA collisions and a useful detection of AA scattering events [5]. It is premature for a joint design study, however, it looked interesting to imagine enlarging the LHeC tracking radius, required also for precision Higgs charm and bottom quark physics, with the possibility to incorporate basically the A3 tracker. It has also been tempting to see whether IP2 can be configured to alternately operate in eh and hh mode while the other experiments, such as ATLAS on IP1, would continue normal hh data taking. At IP2 this would require to keep the two hadron beams and the electron beam close near the beam axis, while previously the non-interacting hadron beam was kept further out. An enlarged radius ep detector design, combined with a new focus on Liquid Argon (LAr) electromagnetic calorimetry, and a concept for such a double use IR are essential parts of this paper.

This article is structured as follows. Section 2 gives an account for the physics programme describing new developments as well as the basic interest for five selected areas, parton structure, top and Higgs physcis, searches for physics beyond the Standard Model (BSM) and in some detail the physics of heavy ions in DIS and combined. Section 3 presents a new default LHeC detector design as indicated above. Section 4 recalls the LHeC characteristics and describes novel optics considerations and a new IR concept, able to accommodate DIS and hh collisions. The paper concludes with a summary in Section 5.

2 Physics with *eh* and *hh* at the LHC

The physics programme at the LHC and the DIS programme at the LHeC are extremely rich and stand on their own. However, they also have much in common: with the necessity of understanding hadron structure and parton dynamics for searches and precision measurements at the LHC, with novel top quark physics and the opportunity to explore the Higgs mechanism at per cent level, further, in the search for new physics and in the understanding of nuclear parton structure and the phenomenon of the Quark Gluon Plasma and heavy ion physis in general. With a view on the resulting detector constraints and for illustrating the exciting physics programme that the LHeC entails, we have chosen these five topics for a brief description of the potential of the ”Experiment for Electron-Hadron Scattering at the LHC” we here describe. Some special emphasis is given to heavy ion physics in view of the idea, mentioned above, of possibly realising this experiment in a configuration that may jointly be used by DIS oriented and more heavy ion interested communities. Similar illustrations of the physics potential and experimental requirements could be provided for the physics at small Bjorken x, for diffraction, electroweak interactions and other areas, see ref. [3]. The discovery of the rise of the gluon and quark densities towards small x at HERA came as a surprise: one should be aware that the opening of an unexplored kinematic range, accessed with so high luminosity, may lead to new surprises and should not pretend to be able to predict everything.

This also regards, technically, the development of analysis tools, for which the past decade on LHC physics brought many examples of results exceeding in their depth and precision the expectations by far. Finally, new theoretical insight or surprises from other particle physics experiments, may indeed shift the focus.

2.1 Partons and Proton Structure

One may distinguish four phases, including the LHeC, of the experimental development of the physics of parton structure of the proton which was opened with the SLAC-MIT lepton-hadron scattering experiment at Stanford in 1968: fixed target experiments, HERA, *pp* Drell-Yan scattering and the LHeC. The role of a next, luminous energy frontier *ep* scattering experiment becomes obvious when one revisits the past and realises the unique potential of the LHeC, recently presented in much detail [3].

Partons, quarks and gluons, are confined inside the proton; still a major puzzle for modern physics, they cannot be observed directly. The pattern of hadrons can be described with three up-type quarks (u, c, t) and three down-type quarks (d, s, b). For each quark there exists a partner anti-quark. Quarks of any type q have a certain probability of carrying a fraction x of the proton's momentum, described by a momentum density function $xq(x)$, called a parton distribution function (PDF). The characteristics of the proton are given by the valence content of two up and one down quarks. The relative distribution of the proton's momentum among the quarks varies with x. It changes as we resolve the proton more deeply in lepton-hadron deep inelastic scattering, i.e. through a virtual photon or a Z or $W^{\pm}$ boson, of virtuality Q^2, interacting with a quark. The strong interaction between quarks is mediated by gluons, discovered in 3-jet events in e^+e^-, which carry a half of the proton's momentum. The quark-gluon interactions are described within QCD, with a coupling constant $\alpha_s(Q^2)$. With rising Q^2, the coupling decreases logarithmically such that asymptotically quarks become free and the strong interaction at the parton level can be described as a perturbation theory. These and further fundamental properties have been established[1] in a first era of PDF physics enabled by a series of neutrino, electron and muon scattering experiments on stationary hadronic targets.

[1] Despite their phenomenological success there continue to exist certain doubts about the whole parton picture based on principles for the structure of nature going back to Newton [85] with testable hypotheses at the LHeC, which therefore has been termed the "Newtonian Telescope of CERN".

HERA was the first *ep* collider. It extended the kinematic range of DIS experiments, given as $s = Q^2_{max} = 4E_eE_p$, by two orders of magnitude but fell short against those by again about two orders of magnitude in luminosity. Its contributions to the understanding of parton structure and dynamics, nevertheless, can not be underestimated. Of special importance has been, firstly, the extension of DIS into the very high Q^2 region with a) the validation of the linear DGLAP evolution law to Q^2 values beyond the weak boson masses, $10^4\,\mathrm{GeV}^2$, and b) the simultaneous use within one experiment of the charged (CC) and neutral current (NC) weak interaction, besides the electromagnetic NC photon exchange, to determine PDFs, including first determinations of the charm and bottom quark densities through impact parameter measurements. Since the accessible x range towards small x is extended $\propto 1/s$, HERA was able to resolve, in addition, the gluon, sea and valence quark behaviour at small x. It established the dominance of xg at small x but could not convincingly answer the question of whether non-linear gluon-gluon interactions occur, which would damp the rise of xg towards small x and lead outside the validity range of the DGLAP equations. The HERA NC and CC collider data did permit a first and far reaching set of PDFs to be determined without using extra data with their own uncertainties [45], and they are the inevitable part of any modern PDF determination.

Following HERA, with the advent of the LHC and its Drell-Yan measurements, the art of extracting PDFs from so-called global data has become an active field of particle physics, to test QCD and to understand LHC measurements using maximum suitable data, and novel analysis and mathematical methods. Such analyses carry a number of severe theoretical and practical difficulties which, despite impressive successes by the various PDF analysis groups, lead to a principally unsatisfactory situation due to the nature of hadron-hadron scattering with respect to DIS, the effect of hadronisation and reconstruction arbitrariness in jet data, the incompatibility of many data sets leading to the rather ad-hoc inflation of uncertainty bands or even exclusion of the most precise data, such as the ATLAS inclusive W,Z data from CT18, for example. A reflection of these effects is the observed difference between PDF sets of different groups which is often larger than the claimed precision of fits. A conceptual difficulty is the uncertainty at high mass, corresponding to large $x \geq 0.5$, where the occurrence of new physics is possible, such that the LHC data should be excluded from PDF fits. The current status of the determination of α_s to about 2 % uncertainty limits the PDF determination, and the precision of predictions such as the $gg \to H$

production cross section being $\propto \alpha_s^2$. Simulation studies on future PDF determinations from the LHC assume that the data compatibility problems may disappear, while the principal problems will in fact remain.

A precision physics era at the HL-LHC will be maximally precise if it was accompanied by the LHeC PDF programme, which is the fourth phase of PDF physics ahead. As described in detail in [3]: i) the increased energy will make the CC DIS data for the first time a useful base extending over 4 orders of magnitude in x and Q^2; ii) all PDFs, $xq(x,Q^2)$ and $xg(x,Q^2)$, can be determined in a single DIS experiment over many orders of magnitude, with $q = u_v,\ d_v,\ u,\ \bar{u},\ d,\ \bar{d},\ s,\ c,\ b$ and also t; iii) the kinematic range, unlike at HERA or lower energy fixed target or ep collider experiments, extends to such low values of x in the DIS region that one will be able to settle the question of non-linear gluon-gluon interactions, etc. An unprecedented precision on these distributions is in reach, as has been simulated more than once but conclusively in [3], including per mille accuracy of α_s. This will comprehensively test pQCD and the underlying parton dynamics view at the highest level; will enable new physics, possibly occurring in the high mass tails from interference contact interaction effects, to be discovered at LHC; lead to possible discoveries in QCD such as the breaking of factorisation not only in diffraction; and enable precision electroweak and Higgs physics at the joint ep/pp LHC facility to a stunning level of precision.

Such an ambitions programme, including precision measurements of the strange, charm and bottom quark distributions and of the longitudinal structure function $F_L(x,Q^2)$, sets important constraints for the experiment here presented: i) it is very desirable that such data exist while HL-LHC operates. Therefore a dedicated study [3] has been made of the LHeC PDF prospects for an initial data set of $50\,\mathrm{fb}^{-1}$, see Fig 1. Such a luminosity is a factor of 100 larger than that which H1 collected in its 15 year lifetime, while being expected in the first LHeC running period [44]; ii) the detector acceptance should extend maximally to small hadron final state angles to cover larger x and to low electron scattering angles to cover low $Q \sim 1\,\mathrm{GeV}^2$, even when one can extend the region of acceptance considerably with lower beam energy runs; iii) hermiticity of the apparatus is required to apply an $E - p_z$ balance criterion which diminishes the radiative corrections dramatically; iv) cross calibration of the hadronic and electromagnetic calorimeter as well as polar angle measurements should ensure a below per cent level accuracy of the energy scales keeping the experimental scale uncertainties small; iv) high resolution hadron energy measurements are required especially for heavy flavour reconstruction, together with impact parameter resolutions of order $10\,\mu$m resulting from novel tracking technology and the small beam size of about $7\,\mu$m transversally, twenty times better than at HERA; v) the large photo-production background shall be tagged, for its own physics study and for substracting it in DIS measurements. A major demand in ep scattering is the control of halo and synchrotron radiation backgrounds through a carefully designed interaction region, see Sect. 4.3. Further experimental requirements are discussed in Sect. 3.1.

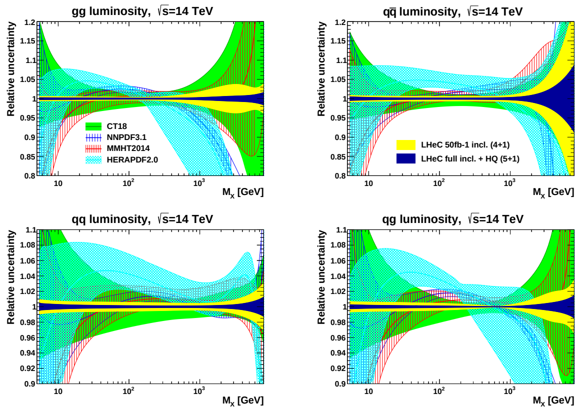

Fig. 1 Expected precision for the determination of parton-parton luminosities as function of M_X in Drell-Yan scattering at the 14 TeV LHC. Light blue: HERA, yellow: initial LHeC run, dark blue: full LHeC data set, green: CT18. For more information see [3]

2.2 Top Quark Physics

Electron-proton colliders at high energy are ideal to study the electroWeak interactions of the top quark. The LHeC is an outstanding single top facility in its own right. The charged current cross-section stands at 1.9 pb, compared to 0.05 pb of the photo-production of $t\bar{t}$. This provides an opportunity to measure the Wtb coupling with high precision and to search for anomalous contributions in the Wtb vertex [6]. With $100\,\mathrm{fb}^{-1}$ of integrated ep luminosity relative errors of order of 1% can be achieved in the measurement of the Wtb coupling. The Next-to-Leading Order (NLO) corrections to the total and fiducial cross-sections are known [7] and do not significantly affect the ability of the LHeC to achieve precision. These may reduce the expected fiducial cross-section of single top production by 14%, while providing stability against scale variations. By contrast, measurements of single top production at the LHC are hampered by the large $t\bar{t}$ production cross-section. This is an epitome of the complementary of the LHeC with the LHC.

Given the level of precision characteristic to the LHeC, other elements of the CKM matrix are also accessible with a precision superior to that of the LHC [8, 9]. Competitive measurements of V_{td} and V_{ts} could be performed at the LHC with ≈1 ab^{-1} of integrated luminosity.

The photo-production of $t\bar{t}$ provides a window of opportunity to measure the $t\bar{t}\gamma$ magnetic and electric dipole moments [10]. Here an energetic photon couples only with the top quark so the cross-section depends directly on the $t\bar{t}\gamma$ coupling. The sensitivity of the LHeC here is superior to measurements of the $b \to s\gamma$ transition and that of the production of $t\bar{t}\gamma$ at the LHC.

The LHeC also provides access to Flavor Changing Neutral Current (FCNC) processes driven by the γtq and Ztq vertexes, where $q = u, c$ [11,12]. This is achieved by measuring the process $e^-p \to e^-W^{\pm}q + X$. The expected sensitivity improves on current limits from the LHC by up to one order of magnitude in case of the γtu coupling, and is competitive with expected accuracies from the HL-LHC.

In addition, important measurements of top quark properties, such as of top quark spin and polarisation [13], and of the top quark mass, for example by measuring the boosted top quark jet in single top quark production.

2.3 Higgs boson Physics in ep and pp at the LHC

As discussed in section 2.2, the LHeC is a single top facility. The cross-section for the production of the Higgs boson in association with a single top is sufficiently large for measurements to be effected. In the SM, the production of the Higgs production in association with a single top is heavily suppressed due to negative interference. As such, it is very difficult to access this production mechanism at the LHC.

The LHeC provides a unique opportunity to study the CP structure of the Higgs boson Yukawa coupling [17]. One can introduce CP-phase ζ_t of the tth coupling, where $\zeta_t = 0$ corresponds to the SM. Thanks to the strong enhancement the $pe^- \to \bar{t}h\nu_e$ for $\zeta_t > 0$, strong limits can be set on deviations from the SM.

Assuming the Yukawa coupling to have the same structure as in the SM, the coupling size could be measured at the LHC with an accuracy of 17% with 1 ab^{-1} of integrated luminosity [17]. The use of multivariate techniques and additional channels not studied so far, the accuracy of the measurement could be improved further.

2.4 Beyond the Standard Model Searches

The clean environment of high-energy electron-hadron collisions provides an excellent framework for studying many extensions of the Standard Model. The excellent detector performance, the absence of pileup, and the large luminosity allows testing of entire classes of models that are difficult to study at the LHC. Many studies from recent years have been summarised succinctly in chapter 8 of ref. [3].

Prominent examples among these studies are searches for sterile neutrinos, for instance via lepton-trijets and displaced vertex signatures [18], heavy scalar particles with masses around the electroweak scale [19], and in general models with final states that look like 'hadronic noise' in proton-proton collisions [20, 21].

Recent studies demonstrate that the LHeC could be a world-leading laboratory to study flavor-changing neutral currents in the charged lepton sector, in particular for processes that lead to electron-to-tau transitions, where the projected sensitivity could be an order of magnitude better than current and planned experiments in tau factories [22].

Scalar and fermion $SU(2)_L$ triplets can explain the observation of neutrino masses via the so-called type-II and type-III mechanisms, respectively. Both types of particles can be produced via their gauge interactions in vector boson fusion, but studying them at the LHC is very challenging due to the towering backgrounds. The prospects of finding triplet fermions via fat jet final states were shown to be feasible at the LHeC [23]. Triplet scalar searches at the LHeC were discussed in ref. [24].

Certain classes of leptoquarks can be studied at the LHeC if they interact with first generation fermions and have decay channels that are difficult to reconstruct at the LHC. It is possible to test certain explanations of the flavor anomaly $R_{D^{(*)}}$ via the R_2 leptoquark at the LHeC via its decays into τb final states [25].

Less minimal models with a $\tilde{R}_2$ leptoquark that has a dominant branching ratio into right-handed neutrinos may escape the LHC searches, but can be studied at the LHeC Ref. [26]. The specific signature of a displaced fat jet, stemming from the decay of a long lived heavy neutrino, would be a very promising sign of this model at the LHeC [27] and could already be observable within the first few months of operation.

Dark photons with masses below 10 GeV can be tested in a decay-agnostic approach via distinct non-dglap scaling violations, which may be the smoking gun for LHeC searches [28]. In the event that the dark photon in this mass range is long lived and decays dominantly to lepton pairs, LHeC searches for displaced dark photon decays would be sensitive to an otherwise challenging region of the parameter space [29].

2.5 Heavy Ion Physics

The physics opportunities provided by the availability in the same detector of DIS off nuclei, proton-nucleus and nucleus-nucleus collisions, eA, pA and AA respectively, are immense (see e.g. the discussions in [31] and refs. therein):

– On the one hand, as extensively discussed in [1,3], eA collisions at high energies at the LHeC will reveal the partonic structure of nuclei and the QCD dynamics in unexplored kinematic regions hitherto of high energies and parton densities. This is the region of relevance for pA and AA collisions at the LHC and beyond.

– On the other hand, the proposed heavy-ion (HI) detector to be installed in IP2 during LS4 to operate during subsequent LHC Runs [4] aims to provide outstanding tracking capabilities in the soft region down to tens of MeV and, due to fast timing, large possibilities for PID beyond dE/dx [30], and to be able to work and record minimum bias collisions at the largest AA achievable luminosity.

– The combination of this outstanding tracking, extended to ~ 1 degree in the backward and forward directions and providing particle ID in the soft sector, with EM and hadronic calorimetry and muon detection makes it a general purpose detector for pp, pA and AA collisions, with larger capabilities for QCD than ATLAS and CMS and larger acceptance than LHCb.

Such detector will be ideal to explore the new possibilities for physics with ions after LS4 discussed in [32] as, for example, the larger luminosities provided by ions lighter than Pb (O, Ar, Kr) to analyse the presently least understood stage of hadronic collisions, the initial one [33,34], using hard probes. In the following we elaborate on such possibilities.

a. Nuclear structure:
The kinematic $x-Q^2$ extent to be explored at the LHeC and during future pA Runs at the LHC is shown in Fig. 2 and compared with that of the set of data used in present analyses of collinear nuclear parton densities. LHC data will cover most of the kinematic region also covered by the LHeC (note also that the region between the lower and upper hatched regions in brown can be analysed by DY studies at LHCb), but the extraction of nuclear parton densities in pA and AA collisions relies on the validity of collinear factorisation down to rather low values of x and transverse momenta where other dynamics beyond leading twist perturbative factorisation could be at work. These new dynamics are strongly suggested by the finding at the LHC that many observables in pp and pA behave in a similar manner to that in AA, where they are interpreted as signatures of the existence of the Quark-Gluon Plasma (QGP) – the *small system problem*, see [40] and refs. therein. Besides, even assuming collinear factorisation to hold, the sensitivity to different flavours varies strongly when moving in the kinematic plane.

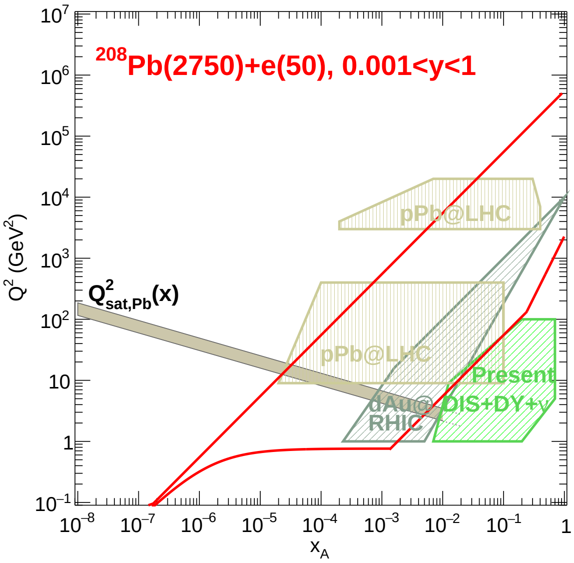

Fig. 2 Kinematic plane studied in ePb collisions at the LHeC ([3], solid red lines) together with the regions explored in present analysis [35]: DIS and DY fixed target data (hatched area in green), hadron production in dAu collisions at RHIC (hatched area in grey) and Run 1 dijet and EW boson studies in pPb collisions at the LHC (hatched upper region in brown). Also shown in the hatched upper region in brown are the expectations from dijets in Run 2 [36] and from EW bosons in future Runs [32], and in the hatched lower region in brown the expectations from Run 2 D-meson analyses [37] and from DY and photon studies in future LHC Runs [32,39].

DIS offers fully constrained kinematics through the reconstruction of the electron angle and energy, a cleaner theoretical environment where factorisations can be proven [41] and perturbative calculations and resummations can be pushed to very high orders, and the possibility of full flavour decomposition through the combination of NC and CC and heavy flavour tagging. As shown in [1,3], these opportunities will be fully exploited at the LHeC, where the nuclear PDFs can be determined with unprecedented precision without requiring prior knowledge of proton PDFs.

Factorisation schemes exist beyond collinear factorisation, such as high-energy factorisation, TMD,... [41], and, eventually, the breaking of linear evolution when parton densities become high enough with decreasing x or increasing mass number of the colliding objects. Our current understanding of non-linear QCD dynamics views them as density effects, making both ep and eA essential input to check such explanation. The combination of inclusive, diffractive and exclusive (vector mesons and photons) studies at the LHeC [1,3] will establish the correct factorisation and dynamics in the different kinematic regions. Then, with the relevant non-perturbative information (PDFs, GPDs, TMDs,...) available, the validity of the corresponding factorisation will be checked in pA [32], thus elucidating the mechanism of particle production in high-energy nuclear collisions.

Finally, the possibility of accelerating ions lighter than Pb will clarify the dependence of parton densities on the mass number. Therefore, it will eliminate the need of interpolations, based on assumed factorisation of the mass number dependence, between different nuclear species in global fits. This will greatly reduce the theoretical uncertainties inherent to the interpolation procedure.

b. Soft physics:

The proposed HI detector [4] to be installed in IP2 offers large possibilities for measurements in the very low transverse momentum region. For example, dileptons whose spectrum may be sensitive to the restoration of chiral symmetry at high temperatures, very low energy photons (with spectra strongly influenced by the dynamics at the initial stage) via conversions, coherence in pion production (due to Bose-Einstein condensation),... Such detector will also provide high precision measurements of collective features like azimuthal asymmetries. The possibility to run different nuclear species will also allow for disentangling the dependences on total number of participating nucleons from those of collision geometry: one will have access to collisions where, for different nuclei, one has the same total number of participating nucleons but different collision geometry, and same geometry with varying number of participants.

While the standard description of these collective features [40] is done in the framework of relativistic hydrodynamics, and the comparison with data used to extract QGP properties, it is known that hydrodynamics works well in out-of-equilibrium situations. In fact, it is currently believed that hydrodynamics is the long wavelength limit of quantum field theories. How this macroscopic description emerges from the microscopic QCD dynamics off the highly out-of-equilibrium initial conditions is the hottest topic in the field. To clarify this, it is crucial to establish the proper factorisation at work in pp, pA and AA collisions at high energies and the dynamics in the initial stages prior to the application of hydrodynamics. It is here where the contribution from ep and eA collisions in similar kinematic regions – at the LHeC – becomes crucial, as DIS is the ideal system to elucidate these aspects. It will also contribute to reduce the uncertainties in the extraction of QGP properties from the comparison of data with hydrodynamic calculations, those coming the initial conditions and the initial stage dynamics [42].

c. Hard probes:

Among the hard probes, heavy-quarkonium production processes have always been a subject of special interest in high-energy physics. They involve both perturbative and nonperturbative aspects of QCD, corresponding to the production of the heavy-quark pair and its non-perturbative evolution. In addition to the hadronic experiments, the LHeC provides a helpful tool for the study of electro and photo production of quarkonium. These processes, which involved a highly virtual photon for electroproduction or a real one for photoproduction, provide unique opportunities for the study of the quarkonium production mechanism and the perturbative QCD calculation reliability. Moreover, the high-gluon densities involved in these processes offer the opportunity to have an insight into the gluon generalized parton distribution in nuclei, the role of color correlations, and the color-dipole nature of quarkonia. At low transverse momentum, the proposed HI detector [4] at IP2 will offer the possibility to study separately the prompt and non-prompt quarkonium production with the identification of the contribution from excited states by detecting low energy photons. Such separation will allow a better characterisation of the QGP [43], based up to now on the anomalous nuclear dependence of quarkonium hadroproduction. Besides, the capabilities of the detector can have a great impact on the field of hadron spectroscopy, opening the possibility to measure the photoproduction of X, Y, Z states. Such studies demand an understanding of the production mechanism of quarkonia which presents large uncertainties until now, and of the effects of conventional, cold nuclear matter on quarkonia yields, both of the nuclear modification of parton densities but also of possible absorption or final state effects. Note that quarkonia are suppressed also in pA collisions, which constitutes one of the pieces of the small system puzzle. eA collisions at the LHeC, with the possibility of varying the nuclear species, will be complementary, contributing amply to clarify all these aspects. The addition of muon detection capabilities to the proposed new HI detector will further enhance its potentialities in all these aspects.

A completely new subject to be added to the physics program of the proposed HI detector is the physics of high transverse momentum particles and of jets – named *jet quenching*, usually employed in HI collisions as tools to analyse the QGP properties [46] but of great interest in QCD and SM and for searches of BSM. The addition of calorimetry and of muon detection to the superb tracking will open numerous possibilities for studies of jet substructure, hadrochemistry and EM radiation within jets, heavy flavoured tagged jets, etc. It is to be noted that jet quenching is the only observation in HI that has not been found in small systems. eA collisions at the LHeC offer the opportunity to study the influence of nuclear matter on jets [47], with abundant yields at high transverse momentum [1], thus contributing to the understanding of the small system puzzle and of the physics of jets for their use in HI collisions. A related subject is the use of high transverse momentum particles and jets to understand the initial stage of hadronic collisions [33,34,48], an aspect that will benefit greatly from the possibility of varying the nuclear size of the colliding hadrons which provide larger centre-of-mass energies and luminosities [32].

d. Ultraperipheral collisions:

Ultraperipheral collisions (UPC), in which one or both of the colliding hadrons act as sources of large fluxes of quasi-real photons, are a hot topic at the LHC [49]. They offer the possibility of studying photoproduction, being in that sense complementary to DIS in which the photon virtuality can be controlled and varied. They have been exploited until now through studies of exclusive vector meson production and dijets with the aim studying nuclear PDFs, and of dimuons and of two-particle correlations in the search of collective effects in systems smaller than pp[2]. UPC have also been used to study light-by-light scattering [51]. All these possibilities can be further exploited in a new detector which besides tracking, calorimetry and muon detection, will be provided by photon, electron, proton and nucleus detection in the very backward and forward regions. eA offers similar opportunities in a more controlled setup, with the additional possibility of further constraining the photon distribution inside the electron, see e.g. [52] and refs. therein. Further, the determination of the nuclear PDFs in inclusive processes in eA would verify the numerous assumptions underlying their extraction in UPC.

[2]In this respect, the ATLAS Collaboration claims the observation of azimuthal asymmetries [50] in γPb collisions.

3 Detector

The LHeC detector, as a modern general purpose ep detector, is a composite system made of several subcomponents: beampipe, tracking, calorimetry, magnets and a muon system, each optimized for its purpose and adapted to the interaction region, which has the peculiarity of hosting 3 beams, the 2 proton or ion beams, of which one is a spectator while the other one is interacting with the counter-rotating electron beam.

In the following section the LHeC detector baseline design and some of its subcomponents are discussed illustrating few aspects and recent developments. Some consideration to adapt the detector for higher energy running (HE-LHC or FCC) or with ion-ion collisions are briefly addressed. Further detailed information can be found in the CDR [1], and its recent update [3].

3.1 Requirements

The detector should be highly hermetic in order to maximize coverage, in both the forward and backward directions, to provide a precise measurement of scattered electrons towards very low-Q^2 and of the hadronic final states. For charged current processes, the reconstruction of kinematic variables is only possible through hadronic final state measurement and excellent performance on calorimetry for hadrons is desirable to reconstruct the missing energies. The good hermeticity is also important for calibration of the detectors through transverse momentum balance using NC DIS and photoproduced dijet events.

Fine segmentation and good resolution for the electromagnetic calorimeter is required all over the angular coverage to tag both low-Q^2 and high-Q^2 neutral current events. Good resolution in the hadronic section is also important to measure the missing energies for CC DIS as well as for QCD studies using jets.

Excellent flavour tagging performance is desirable, especially in the forward direction, for flavour decomposition of jets and for tagging the SM Higgs decaying to $b\bar{b}$ and $c\bar{c}$, which are predominantly produced in large η (positive Z is defined as incoming hadron beam direction for ep/eA collisions).

There are also various constraints and consideration to take in to account from the accelerator and technical aspect of detectors:

- The detector shall have a magnet system consisting of one central solenoid along with a dipole system to steer the electron beam allowing for head-on collisions at the interaction point;

– The non-interacting proton/ion beam has to bypass the *ep* interaction yet to be guided through the same beam pipe housing the interacting electron and proton/ion beams;
– The shape of the beam pipe has to allow for the synchrotron fan to leave the interaction region unaffected and with minimal back-scattering;
– Good vertex resolution implies a small radius and thin beam pipe optimised in view of synchrotron radiation and background effects;
– The tracking and calorimetry in the forward and backward directions have to be set up to take into account the extreme asymmetry of the production kinematic with multi-TeV energies emitted in the proton beam direction (forward) and electromagnetic and hadron energies limited by the electron beam energy backwards;
– Very forward and backward detectors have to be set up to access the diffractive produced events and tagging photo-production besides measuring the luminosity with high precision, respectively.

These and further specific requirements from inclusive DIS, see Sect. 2.1, are basically known from the H1 and ZEUS experiments at HERA. However, at the LHeC they are posed with extra severity because of the much enlarged beam energies, wider physics programme and more ambitious precision demand driven by physics and enabled with a hugely increased luminosity as compared to HERA . Some of them can be easier fulfilled for the high interaction rate will illuminate the complete detector with high statistics, an essential ingredient for cross-calibration of its parts.

3.2 A Detector for DIS at the LHC

The present LHeC detector is illustrated in Fig. 3. The LHeC detector is asymmetric in design, reflecting the beam energy asymmetry. The design is largely based on established technologies from the LHC general purpose detectors, ATLAS and CMS, while more advanced technologies are utilised to fulfill the above described requirements and to adopt to different running condition. The detector covers the angular range from 1° to 179° by the calorimeters to achieve the required hermeticity. Compared to *pp* running, the expected *ep* collision rate is about 3 orders of magnitude smaller relaxing somehow the requirement on radiation hardness and also data acquisition. The pile-up rate is less than 0.1 per crossing at the LHeC for $10^{34}\,\mathrm{cm}^{-2}\mathrm{s}^{-1}$. The neutron field also expected to be a few order of magnitude smaller than the LHC environment.

As illustrated in Section 4.5 (Fig. 13) a dipole field is needed to steer the electron beam in the interaction region and allow for head-on collisions with the proton beam. The required dipole field (0.17 T over the range $z = [-8\mathrm{m},\ +8\mathrm{m}]$) is combined in the central region with the central solenoid providing a field of 3 T. The synchrotron radiation generated by the electron beam in the dipole field is leaving the interaction region not affecting the detector performance thanks to the asymmetric design of the lightweight beryllium beampipe.

The generic detector consists of, from the interaction point to the outer direction, the silicon tracker (the central barrel part, forward and backward wheels, respectively); the electromagnetic calorimeter housed inside solenoid and dipole magnet; the hadronic calorimeter and the muon system. Not shown in the figure are backward (electron-side) detectors for low-angle scattered electron to tag γp and γA collisions and forward detectors for neutrals (n, π^0 ...) from the p/A remnant and protons spectrometer to measure proton momentum from elastic and quasi-elastic scattering.

This baseline design serves also as as generic configuration for HL-LHC and FCC-he where the main changes to be made for higher collision energy are the extensions for rapidity coverage in the tracking system and the depth (X_0, λ_I) in the calorimetry; both affecting mainly the size of the detector in the beam direction, but only logarithmically. With respect to the earlier versions presented in the CDR and in the update, some optimization has been done in particular to the silicon tracking and to the calorimetry which are described below in more detail. The larger tracking volume with longer lever arm measurement and more track points allows for better resolution even at a slightly reduced B field. We expect that this configuration will deliver good and stable performance also in different experiment and accelerator configurations (*eh* and *hh* running).

3.2.1 Silicon Tracking System

As described previously, excellent flavour tagging ability, including charm quarks, is required across wide angular range, in particular towards forward rapidities. The decay particles from the SM Higgs may go beyond $|\eta| > 2.5$, the usual tracking coverage for the LHC *pp* detectors. The silicon tracker is shown in Fig. 4. It covers up to $|\eta| < 3.6$ with at least six hits and two hits for $-4.3 < \eta < 4.8$, with extended sections of disk wheels (seven for forward and five for backward). In comparison to earlier LHeC tracker the outer radius was extended from 60cm to 80cm and the number of layers in the barrel region from 7 to 10 layers while the mag-

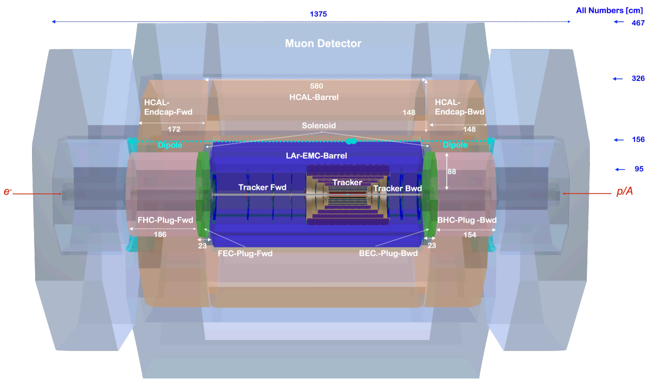

Fig. 3 Side view of the updated baseline LHeC detector concept, providing an overview of the main detector components and their locations. The detector dimensions are about 13m length and 9m diameter. The tracker is setup using pixel, macropixel and strip detectors. The barrel elctromagnetic LAr-calorimeter EMC (in blue) surrounding the tracking region. The solenoid magnet is placed at radii immediately outside the EMC-Barrel, and is housed in a cryostat, which it shares with the weak dipole magnet that ensures head-on collisions. The hadronic calorimeter HCAL in the barrel part (colored orange; it uses steel & scintillating tiles) is located outside of the solenoid. The forward/backward electromagnetic calorimeters FEC/BEC (in green) and hadronic calorimeters FHC/BHC (in bright orange) are using Si-based sensitive & readout technology and as absorbers W/Pb and W/Cu, respectively [1,3]. The muon detector (in grey) forms the outer shell of the detector. The detector description has been setup using **DD4hep** [53].

netic field of the solenoid was reduced from 3.5 T to 3 T. Using the **tkLayout** tool [56] for optimising the tracker arrangement and minimising the material impact over a large region of η, the calculated radiation length figure shows tolerable levels Fig. 5. Some properties of the tracker setup are summarised in Tab. 1.

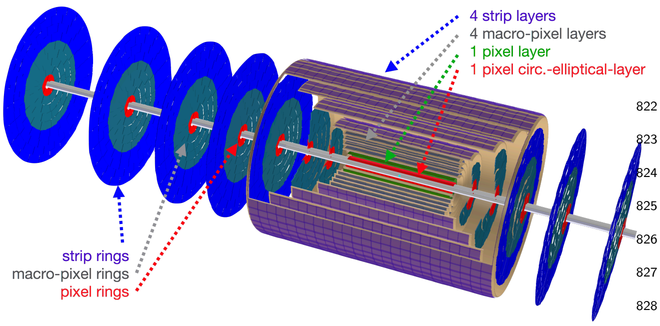

Fig. 4 The full Silicon central tracker for the LHeC.

The relatively small radiation level allows to employ CMOS-based technology for the inner silicon tracker. Depleted CMOS sensors, also known as Depleted Monolithic Active Pixel Sensors (DMAPS), are position sensitive detectors in industry standard CMOS or High-Voltage-CMOS (HV-CMOS) processes [67]. These sensors are extremely attractive for experiments in particle physics as they integrate the sensing element and the readout electronics in a single layer of silicon, which removes the need for interconnection with complex and expensive solder bump technology. Depleted CMOS sensors also benefit from faster turnaround times and lower production costs when compared to hybrid silicon sensors. The final choice will depend on the region of exploration. Low-fill factor DMAPS have been or are being prototyped and produced for several experiments in particle physics, such as Mu3e [68], ATLAS [69], LHCb [70], CLIC [71] and ALICE [4,30] in a few different processes. Today's most performant DMAPS detectors are 50μm thin and have 50μm x 50μm cell size with integrated mixed analogue and digital readout electronics, 6ns time resolution and 2×10^{15} 1MeV neq/cm^2 radiation toler-

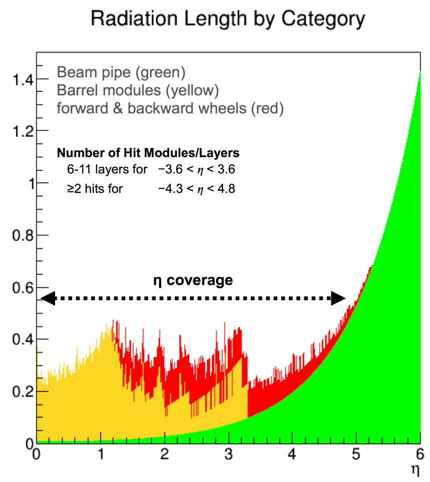

Fig. 5 Tracker simulation/optimisation using **tkLayout** [56]. Support structures and services are not included.

Table 1

LHeC Tracker Part		η_{max}	η_{min}	#Layers$_{\mathrm{Barrel}}$
Inner Barrel	pix	3.3	-3.3	2
	pix$_{macro}$	2.	-2.	4
	strip	1.3	-1.3	4
				#Rings$_{\mathrm{Wheels}}$
End Caps	pix	4.1/-1.1	1.1/-4.1	2
	pix$_{macro}$	2.3/-1.4	1.4/-2.3	1
	strip	2./-0.7	0.7/-2.	1-4
Fwd Tracker	pix	5.2	2.6	2
	pix$_{macro}$	3.4	2.2	1
	strip	3.1	1.4	4
Bwd Tracker	pix	-2.6	-4.6	2
	pix$_{macro}$	-2.2	-2.9	1
	strip	-1.4	-2.5	4
Total $\eta_{max/min}$		5.2	-4.6	

Summary of the main properties of the tracker modules in the revised LHeC detector configuration based on calculations performed using tkLayout [56]. $\eta_{max/min}$ denotes the pseudo-rapidity range. #Layers$_{\mathrm{Barrel}}$ are the number of layers in the barrel and #Rings$_{\mathrm{Wheels}}$ the number of wheels in the End Caps, Fwd and Bwd tracker parts, respectively.

ance. The development is ongoing and extends towards radiation hard technologies. Interesting for our purpose are the possibilities of features offered by CMOS imaging sensor technologies, called stitching, which allows developing a new generation of large size MAPS using wafers that are 300mm in diameter. Moreover, the reduction of the sensor thickness to values of about 20-40μm shall allows for exploiting the flexible nature of silicon to implement large-area curved sensors. In this way, it becomes possible to build cylindrical or in general curved layers of silicon-only sensors, with a significant reduction of the material thickness by avoiding overlap between sensors [38, 54, 55].

The new accelerator optics for concurrent running of ep/eA and pp, AA running, respectively, steers the beam such that the interacting particles collide at the same vertex point (see 4.6). Thus the IP2 could house a multipurpose detector serving for all those physics programs related. The advantage for cross-calibration of dedicated physics searches is obvious.

The challenge in vertexing at the LHeC is that the beampipe has to be extended in order to accommodate the synchrotron radiation fan from the electron beam. To minimise the impact, the innermost barrel pixel layer is designed to follow an optimized circular-elliptic shape of the beampipe as shown in Fig. 6. Thanks to the integrated read-out electronics of the DMAPS sensors, the layout of the innermost layer can be flexible. Currently using a scheme with many narrow sensors in x - y coordinate plane, see Fig. 6, following the shape of beampipe as closely as possible. A possibility to use the bent sensors as described above is being pursued.

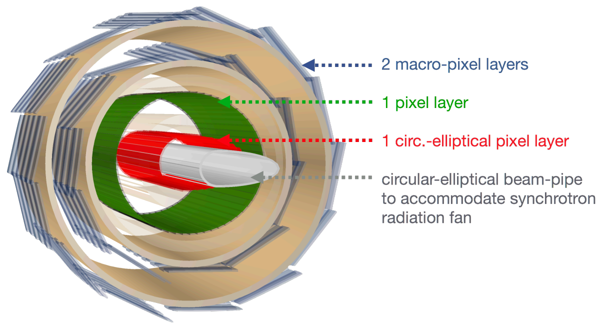

Fig. 6 A view of inner 4 layers of central barrel tracker with innermost circular-elliptical silicon pixel layer following the shape of beampipe.

3.2.2 Calorimetry

As illustrated in Section 3.1, The LHeC requires well developed Electromagnetic and Hadronic sections. The electromagnetic calorimeter surrounds completely the silicon tracker and can be subdivided into a barrel, a forward and a rear system.

For the barrel region two options have been considered: a cold option using Liquid Argon, copper electrodes and lead absorbers, and a warm one based on lead absorbers and scintillator tiles. Liquid Argon is known for its resolution, linearity, long term stability and radiation tolerance confirmed by the use over many years in ATLAS and H1 experiments [72–81]. The cryogenic system required for the LAr option can be combined in the LHeC detector with the one from the Magnet system, which is directly surrounding the calorimeter. The flexibility in the longitudinal and transverse segmentation, and the possibility of implementing a section with narrow strips to measure the shower shape in its initial development, represent additional advantages [80].

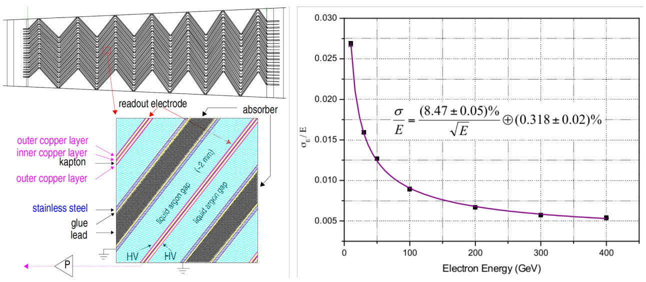

Fig. 7 Longitudinal view of one cell of the ATLAS LAr Calorimeter, showing the accordion structure (left). The LHeC LAr accordion calorimeter energy resolution for electrons between 10 and 400 GeV (the **EMC** simulated using **GEANT4** [82]) (right) [1].

Fig. 7 (left) shows a detail of the accordion-electrode structure. A basic cell consists of an absorber plate, a liquid argon gap, a readout electrode and a second liquid argon gap. The mean thickness of the liquid argon gap is constant along the whole barrel and along the calorimeter depth. The LHeC LAr calorimeter **EMC** would also provide the required energy resolution and detector granularity (Fig. 7 (right)). As an alternative a (warm) option for a lead-scintillator electromagnetic calorimeter has been simulated for comparison. The advantage compared to the LAr-calorimeter are no cryostat walls in front of the barrel **EMC** introducing additional dead material. More details to the LAr-calorimeters proposed can be found in the CDR [1].

The hadronic calorimeter in the barrel part is a sampling calorimeter using steel and scintillating tiles as absorber and active material, respectively, for good resolution. This also provides mechanical stability for the Magnet/Dipole cryostat and the tracking system.

Calorimetry in the forward and backward direction at the LHeC needs very fine granularity for position resolution, good e/π separation through shower shape and also good resolution, especially for scattered electron. The very forward and to a lesser extent the backward parts of the calorimeter are exposed to high levels of particle radiation and must therefore be radiation hard by design. Tungsten (W) is considered as the absorber material, in particular for the forward inserts (electromagnetic and hadronic inserts), because of its very short radiation length. Since the backward inserts have looser requirements, the materials for the absorbers are chosen as lead (Pb) for the electromagnetic part and copper (Cu) for the hadronic. The active signal sensors have been chosen to be silicon-strip for electromagnetic forward/backward calorimeters and silicon-pad for hadronic forward/backward calorimeters. The demanding requirements of very forward/backward angle resolution favors fine segmentations of calorimeter cells interconnecting the tracking and calorimeter information for best particle-tracking and -identification. Those tracking- / imaging-calorimeters based on Si-technology appears to be appropriate to withstand the higher radiation load near the beam-pipe and opens the opportunity to measure the neutral component of particle flow as already demonstrated by developments of the **CALICE** collaboration for the Linear Collider Ref. [83, 84, 86]. The hadronic calorimeter compensation algorithm would profit as well knowing the neutral part of shower development best. The steel structures are in the central and plug calorimetry close the outer field of the central solenoid. The total depth of the electromagnetic section is about 30 radiation lengths on average in the barrel and backward regions. In the forward direction where particle and energy densities are highest the segmentation/granularity will be more detailed and varies with radius and depth. The hadronic calorimeter has a depth of between 7.1 and 9.6 interaction lengths, with the largest values in the forward plug region. For each of the calorimeter modules, the pseudorapidity coverage, the types of the absorber and sensitive materials used, the number of layers, radiation or interaction lengths, and the energy resolutions obtained from **GEANT4** simulations can be found in Ref. [57].

3.2.3 Muon System

Muon identification is an important aspect for any general purpose HEP experiment. In the baseline LHeC detector design the Muon System provides a reliable muon tag signature which, is used in conjunction with the central detector for muon identification, triggering and precision measurements. The detector elements are organized in a near hermetic envelope surrounding the hadronic calorimetry. In terms of technology choices, the options in use in the LHC general purpose experiments [87, 88] and their planned upgrades are adequate for LHeC as since muon background rates are lower. A solution composed of layers of last generation Resistive Plate Chambers (RPC), providing the Level 1 trigger and a two coordinate (η,ϕ) measurement and possibly aided Monitored Drift Tubes for additional precision measurements appears as appropriate [65]. In the baseline design the muon chambers have a compact multi-layer structure, providing a pointing trigger and a precise timing measurement which is used to separate muons coming from the interaction point from cosmics, beam halo and non prompt particles. This tagging feature does not include the muon momentum measurement, but is performed only in conjunction with the central detector.

4 Accelerator Considerations

The design of the machine is described in detail in the updated version of the LHeC design report [57]. It is based on two super-conducting linacs of about 900 m length, which are placed opposite to each other and connected by three return arcs on both sides (Fig.8). A final electron beam energy of 50 GeV is reached in this 3-turn racetrack ERL design. The concept allows to keep the overall energy consumption on a modest level for up to 20 mA electron current. The main parameter list is shown in Tab. 2.

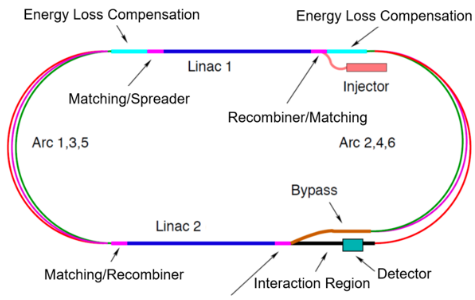

Fig. 8 ERL geometry, using two sc. linear accelerators, connected by return arcs.

4.1 Linac and RF system

The option to design a particle collider as Energy Recovery Linac, provides the opportunity to overcome or avoid a number of limitations of circular machines. In

Parameter	Unit	Value
Beam energy	GeV	50
Bunch charge	pC	499
Bunch spacing	ns	24.95
Electron current	mA	20
trans. norm. emittance	µm	30
RF frequency	MHz	801.58
Acceleration gradient	MV/m	20.06
Total length	m	6665

Table 2 ERL main parameters

order to reach the luminosity of $10^{34}\,\mathrm{cm}^{-2}\,\mathrm{s}^{-1}$ with an electron energy of 50 GeV, the concept of an ERL offers the advantage of a high brightness beam, high beam currents with limited synchrotron radiation losses and it avoids limitations due to the beam-beam effect - a major performance limitation in many circular lepton colliders (e.g. LEP). On the other side, the current of the ERL as well as the emittance are limited by its source. An operational goal of I_e =20 mA for the LHeC has been set, corresponding to a bunch charge of 500 pC at a bunch frequency of 40 MHz. Given three turns for the acceleration and deceleration, an overall current of 120 mA will be circulating in the ERL with impacts on the RF design, facing a virtual beam power of 1 GW. In order to limit RF losses, a super conducting (s.c.) RF system is foreseen with a required quality factor above $Q = 10^{10}$. In collaboration with JLab [58] prototypes have been developed: Figure 9 shows the Q-value of a five cell sc. resonator which lies comfortably above this value up to the required acceleration gradient, which is indicated by the red cursor line in the plot. The vali-

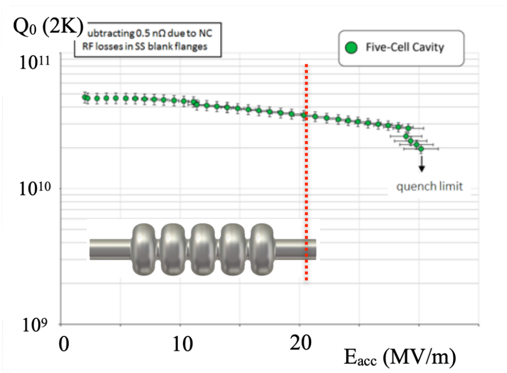

Fig. 9 Q-parameter of the 5 cell cavity prototype

dation of these design concepts and the optimisation of the ERL performance in terms of source brightness and stable and efficient operation in the PERLE facility [59] is a key milestone for the LHeC design.

4.2 Return Arcs and Spreaders

Special care has to be taken in the design of the ERL lattice: The optics of the three return arcs has to be optimised for the different challenges, that come along with the increasing beam energy [60]. At low energy, a flexible momentum compaction lattice will allow optimisation of the bunch length: An isochronous beam optics has been chosen for arc 1,2,3 to allow short bunches. At higher energies, in arc 4,5,6 an efficient emittance control is needed, as the effects of the emitted synchrotron light will take over. These arcs therefore are equipped with a theoretical minimum emittance optics (TME) to mitigate the emittance blow up (see Figure 10). The magnet structure of the linacs has to provide

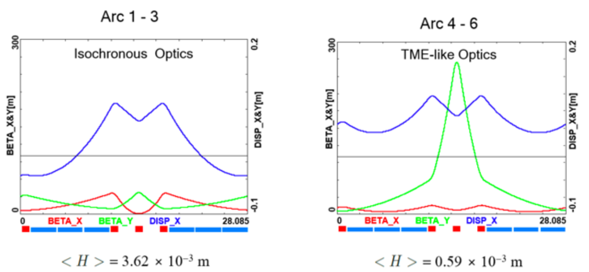

Fig. 10 Basic FMC cells of the ERL arcs: Isochronous (left) for arc 1,2,3 and TME lattice (right) for arc 4,5,6

focusing for the complete energy range of the accelerating / decelerating beams. Here a FoDo structure has been chosen with a phase advance of 130° per cell. Different cell lengths have been investigated and simulation studies showed - not unexpectedly - an increasing performance for a shorter cell length. At the end of the Linac, the beam has to be guided into the return arc that corresponds to the beam rigidity at the given acceleration step. A combination of dipoles and quadrupole magnets provides the vertical bending and adapts the beam optics to the arc structure. This "spreader" (in front) and "re-combiner" (after the arc) represent a non-dispersive deflecting system to provide the necessary vertical off-set between the three arc modules and limit at the same time the detrimental effect on the vertical beam emittance.

4.3 Interaction Region

The Interaction Region (IR) of the LHeC is one of the most challenging parts of the machine: While seeking for highest luminosity in ep-collisions, which includes mini-beta insertions for strong focusing of both beams, the colliding electron and proton beam have to be separated after their collisions and guided to their lattice structures, to avoid parasitic bunch encounters. In addition, collisions and beam-beam effects with the second non-colliding proton beam have to be avoided.

4.4 Proton Beam Optics

The optics of the colliding proton beam follows the standard settings of the HL-LHC. Fig. 11 shows the proton optics at the interaction point of the LHeC. The long-ranging beta-beat which is an essential feature of the HL-LHC optics [61] is clearly visible on both sides of the IP and will be used for both, h-h and e-p collisions in IP2.

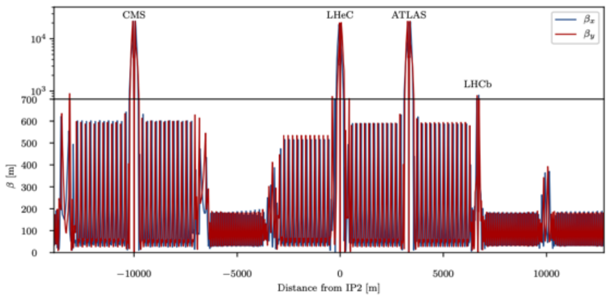

Fig. 11 LHC proton beam optics, optimised for the LHeC design values at the LHeC IP.

Special design effort is needed in the layout of the super conducting quadrupole "QA1": Positioned right after the electron mini beta quadruples, it has to provide sufficient aperture and gradient to re-match the proton optics towards the arc structure. At the same time a field free region inside the cryostat is needed for the outgoing electron beam. Figure 12 shows a first layout of the magnet. The field calculations for both apertures are determined using the magnet design code ROXIE [62] with special emphasis on minimizing the remaining quadrupole field in the electron aperture: located at a distance of 106 mm from the proton design orbit - it has to be low enough not to distort the electron beam. Following the first layout and field calculations described, further R&D will be needed leading to a serious design and construction of a prototype magnet in order to show the feasibility of the technical concept.

4.5 Electron Beam Optics and Separation Scheme

The design orbit of the electron beam - accelerated by the ERL and brought into collision at IP2 - will be merged with the proton orbit only in a short part of the lattice: Due to the different beam rigidities,

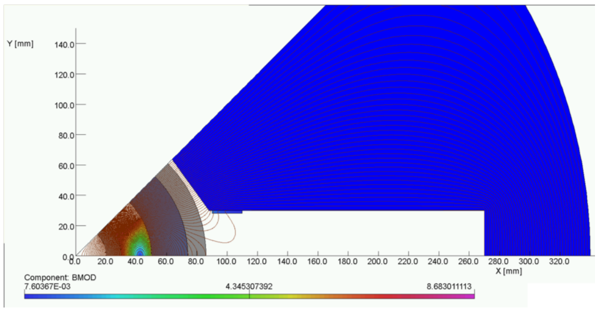

Fig. 12 Layout of the first proton quadrupole after beam separation. Special emphasis is put on minimising the remaining field in the electron aperture at a distance of 106mm from the p design orbit

$$(B * \rho)_p = 23\,333\,\mathrm{T\,m} \qquad (B * \rho)_e = 167\,\mathrm{T\,m}$$

a common focusing structure is not possible. The design of the IR therefore has to take a manifold of conditions into account: Focus the electron beam to the required β values in both planes, establish sufficient beam separation, optimise for smallest critical energy and synchrotron light power, and leave sufficient space for the detector hardware. A separation scheme has been established [63] that combines these requirements in one lattice structure (see Fig. 13). Due to the different rigidity of the beams, a separation is possible through the common effect of several magnetic fields: The spectrometer dipole of the LHeC detector, named *B0* in the figure, is used to establish a first separation. Right after and as close as possible to the IP, the mini-beta quadrupoles of the electron beam are located. They provide focusing in both planes for matched beam sizes of protons and electrons at the IP:

$$\beta_x(p) = \beta_x(e), \qquad \beta_y(p) = \beta_y(e)$$

At the same time they are positioned off-center with respect to the electron beam, thus acting as combined function magnets to provide the same bending field as the separator dipole: A quasi constant, soft bending of the electron beam is achieved throughout the magnet structure: $1/\rho_{B0} = 1/\rho_{quad_f} = 1/\rho_{quad_d}$. Additional conditions were put for a reduced beam size of the electron beam at the location of the first proton quadrupole. At this position, L^*=15 m, the reduced electron beam size leads automatically to a minimum of the required beam separation and as direct consequence to smallest synchrotron radiation effects. The optical functions of the electron beam in this optimised interaction region are shown in Fig. 14.

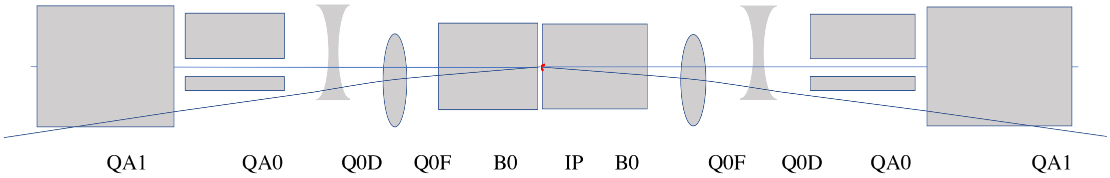

Fig. 13 Schematic view of the combined focusing & beam separation scheme

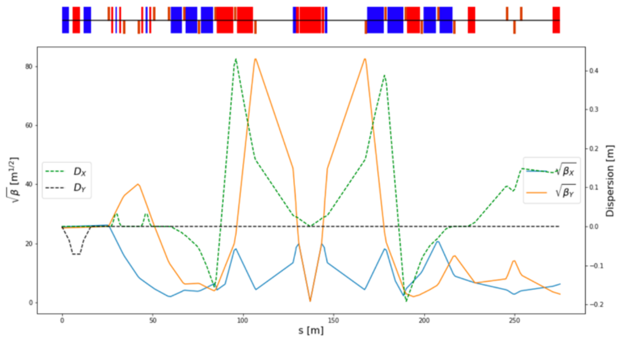

Fig. 14 Optical functions of the electron beam in the IR.

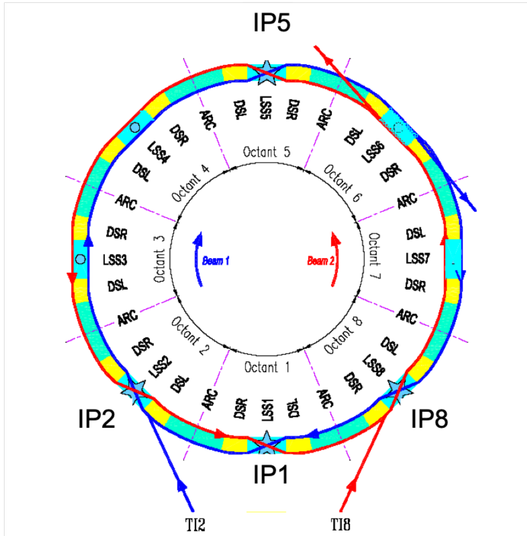

Fig. 15 Geometry of the two LHC beams, crossing from inner to outer ring in the four interaction points IP1,2,5 and 8

4.6 Concurrent eh/hh Operation

The interaction region layout described above has been optimised for highest luminosity, matched beam sizes between electrons and the colliding proton beam and a smooth but efficient beam separation scheme. Still, an additional boundary condition arises from the second, "non-colliding" proton beam: A concurrent operation of the LHeC as electron-proton collider means that the operation as e-p collider will be possible in parallel to the standard LHC proton-proton operation. During e-p operation in IP2, with electrons provided by the ERL, the standard p-p collisions in the LHC interaction points IP1, (ATLAS), IP5 (CMS) and IP8 (LHC-b) will continue and thus the second proton beam has to be guided through the new interaction region IR2, in parallel to the electron and proton beams. At IP2 therefore, in e-p operation mode, the second non-colliding proton beam will be separated by a symmetric orbit bump to avoid direct collisions between the two proton beams as well as with the electron beam. Parasitic encounters with the subsequent bunches are suppressed by a vertical crossing angle. This scenario follows the LHC standard operation, where similar orbit bumps are applied during injection and acceleration phase of the two beams. Additional constraints arise from the need to preserve the overall LHC geometry: The two LHC proton beams will have to cross over from the inner ring to the outer, see figure 15. All in all, two basic operation modes have to be established:

- Standard p-p or h-h collisions in IP 1,2,5,8, no electron beam.
- Concurrent operation of e-p collisions in IP2 and p-p collisions in IP 1,5,8.

Concerning the first operation mode, the set up will be equivalent to the HL-LHC upgrade lattice and optics, with the two hadron beams colliding in all LHC interaction points. The magnets of the electron mini beta structure and beam separation scheme, shown schematically in Fig. 13, will be switched off.
For the second operation mode the colliding proton beam will be focused to match the size and position of the ERL electron beam at the IP. Electron beam focusing and beam separation between electrons and protons will follow the above mentioned scheme. The second non-colliding proton beam however will pass untouched through IR2, but still being used for collisions and data taking in IP 1,5 and 8. For this purpose, a sufficient beam separation between this non-colliding protons and the colliding beams in IP 2 is needed. Schematically the situation is shown in Fig. 16. The beam separation is established via the LHC standard separation bumps, that are used during beam injection and throughout the complete acceleration phase. At the

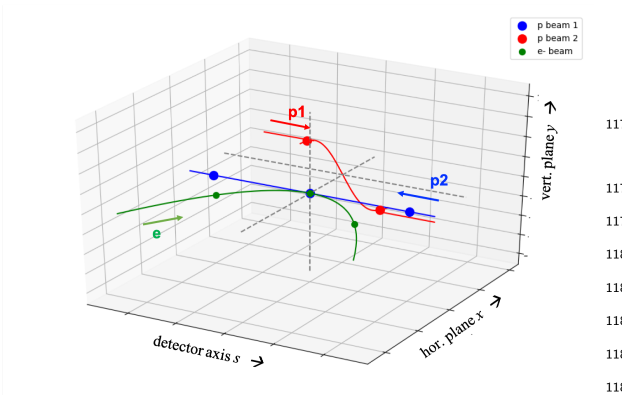

Fig. 16 Schematic view of the three beams in the interaction region. Collisions between electrons and proton beam 1 and a well separated proton beam 2.

interaction point IP2, direct collisions are avoided by a horizontal offset of the non-colliding beam. In addition a vertical crossing angle is applied to prevent effects from the so-called parasitic encounters, that otherwise would occur at a distance of half a bunch spacing (25/2 ns). While this scheme is used during LHC standard operation it requires special attention for the concurrent e-p / p-p operation. A special beam optics for the non-colliding proton beam has to be established, to provide sufficient aperture for this new type of beam operation. The colliding proton beam will be focused strongly to achieve a β-function of 10 cm at the IP. At the same time the non-colliding beam will see a relaxed optics with smallest achievable beam size in the proton mini beta quadrupoles. First estimates, based on an "injection type optics" with β^* of 15 m lead to an additional aperture request of about 10% in the first proton quadrupole Q1A. Further downstream the two proton beams will follow the usual beam separation defined by the separator dipoles D1 and D2 (see Fig. 17). Further studies will concentrate on the level of flexibility of the different LHC magnet lattices which is a pre-requisite for the proposed scenario. Beyond that, the beam-beam effect between the electron and the non-colliding proton beam - traveling for a considerable distance in parallel to each other - will be studied in detail.

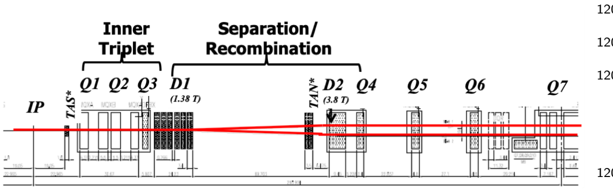

Fig. 17 Schematic view of the LHC proton beam separation scheme. The two separator dipoles D1 and D2 provide the hor. separation needed, before the beams enter their distinct magnet lattices in the arcs.

4.7 Synchrotron Light

The synchrotron light parameters, i.e. critical energy, radiation power and the geometry of the emitted light cone were determined with the simulation code BDSIM [64]. As expected, the synchrotron light conditions in the arcs become more serious turn by turn, reaching the highest level in the return arc 6, after the collision point. The values are summarised in Tab. 3. Special care is needed in the vicinity of the particle detector. The properties of the focusing elements, the separation scheme and the geometry of the interaction region have been optimised for smallest critical energies and power of the emitted light.

Arc	Energy (GeV)	Crit. Energy (keV)	Power (MW)
1	8.75	3.2	0.01
2	17.00	23.9	0.21
3	25.25	78.5	0.75
4	33.5	183.3	2.45
5	41.75	354.8	5.87
6	50.0	609.3	12.17

Table 3 Critical energy and power of the emitted synchrotron light in the return arcs of the ERL.

Fig. 18 summarizes the results. The graph shows the reduction of the critical energy and power in the interaction region, due to the different steps of the optimisation procedure. Starting from a pure separator dipole design to establish the required beam separation, the concept of a half-quadrupole as first focusing element in the proton lattice is introduced as well as an improved beam separation of the electrons by off-centre quadrupoles.

The actual distribution of the detector dipole field and the off-centre quadrupoles has a considerable effect: The red and black points in the graph correspond to the minimum achievable critical energy and emitted power, respectively. Dedicated calculation of the synchrotron light cone and a sophisticated machine detector interface including absorbers will be needed to shield the detector parts and accelerator magnets.

4.8 Beam-Beam Effects

The beam-beam effect will always be the final limitation of a particle collider and care has to be taken, to preserve the beam quality and limit detrimental effects

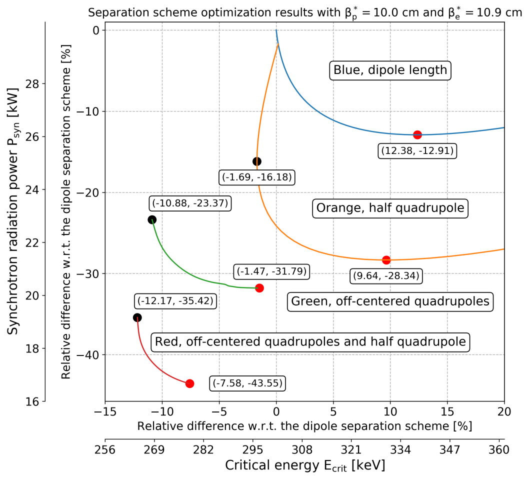

Fig. 18 Optimising the synchrotron light for lowest critical energy and power in the IR, details in the text.

on the emittance to assure a successful energy recovery process in the ERL.

The beam-beam interaction has been simulated with a weak strong tracking simulation for a matched transverse beam size of the electron and proton beam at the IP. In Fig. 19 the situation post collision is represented in the (x,x') phase space.

While tails in the transverse beam distribution as consequence of the beam-beam effect are clearly visible, the core of the beam still remains in a quasi ellipse like boundary. The coordinates obtained are used as starting conditions for the deceleration part of the ERL for a full front-to-end simulation.

The resulting emittance increase and luminosity, taking into account the beam-beam force are summarised in table 4.

Parameters	Optical matching
Luminosity	$8.2 \times 10^{33}\,\mathrm{cm}^{-2}\,\mathrm{s}^{-1}$
$\Delta\gamma\varepsilon$	15 mm mrad

Table 4 Luminosity and transverse emittance growth for the optical matching.

On the other hand, the beam-beam effect on the proton bunch remains in the shadow of the other effects and is considered as not critical. A careful alignment of the electron bunch at the IP however will be necessary as it could lead to undesirable proton emittance growth build up [65].

The phase space distributions of the electrons after beam collision does not follow a Gaussian distribution. The non linearity of the interaction distorts the electrons on the edges as well as modifies the Twiss parameters from the original design as shown in Fig. 19. The distortion of the phase space impacts the particle density and makes the core and tail of the distribution more populated than a Gaussian distribution. Nevertheless, the ellipse fitted to the post-collision distribution, that takes into account the modification of the Twiss parameters at the interaction point - and including a so called capture optics - has a higher central density and the tails are slightly less populated.

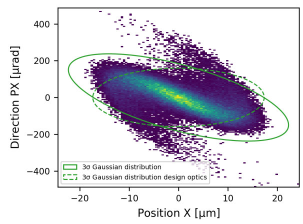

Fig. 19 Phase space of the electron distribution after beam collision, backtracked to the IP for matched optics conditions of electrons and the HL-LHC proton beam.

	Gaussian distribution	Optical matching
1 σ	68.27%	46.28% (70.74%)
2 σ	95.45%	78.40% (95.37%)
3 σ	99.73%	95.76% (98.44%)
4 σ	99.99%	99.24% (99.53%)

Table 5 Comparison of the electron distribution after non linear beam-beam interaction. The values represent the density of electrons for several rms emittance areas for the design optics as well as for the fitted ellipse of the post-collision distribution, in parenthesis.

Further studies are needed regarding the impact of a smaller beam size of the electrons at the IP *e.g.* following the quest for a luminosity optimum. In fact, the optimal separation scheme may need to be adapted, the beam stay-clear aperture in the mini-beta quadrupoles would decrease and could be a showstopper for this luminosity optimisation scheme and finally the use of not matched lepton/hadron beam sizes could lead to instability for the proton bunch.

4.9 Front-to-End Tracking Studies

The tracking simulations of the ERL have been performed with the tracking code PLACET2 [66] and include, beyond the properties of the magnetic fields the Incoherent Synchrotron Radiation (ISR) and the weak-strong beam-beam interaction at the interaction point (IP). The studies focused on the achieved transmission and the beam quality along the ERL passages, *i.e.* the emittance budget required, for different machine circumferences that are considered for the basic machine layout. The beam parameters used for the tracking simulations correspond to the main parameter list as listed in Tab. 2.

The optics design of the multi turn ERL is shown in Fig. 20 and present the sequence of linacs and arcs leading to the interaction region with its strong focusing and accordingly large vertical beta function in the mini beta quadrupoles. The other peaks are located in the matching sections between the linac optics and the periodic arc structure. The tracking takes place over three acceleration turns until the IP. Three deceleration turns are following in the same lattice structure, established via a RF phase shift in the highest energy return arc 6.

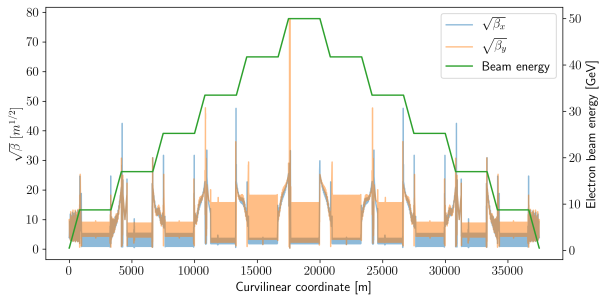

Fig. 20 Representation of the beta functions and the beam energy along the multi-turn ERL operation.

The objectives are: obtain the required transverse emittance at the IP; collide with the proton beam; minimise the emittance growth; taking into account eventual optics mismatch and distortion due to the non-linear beam-beam effect; decelerate the electron beam during the energy recovery process and guarantee minimum particle losses, while the energy spread will reach levels of a few percent in the last deceleration step.

The synchrotron radiation for each ERL circumference that has been studied varies significantly and has a strong influence on the energy recovery efficiency, see the results Tab. 6.

The results of the tracking simulations and the obtained emittance growth during the three turn beam acceleration agree nicely with the analytical calculations. After the interaction region the particles increasingly gain energy spread that creates a deviation from the design optics. The optics mismatch results in an extra emittance growth and ultimately leads to beam losses during the deceleration phase. The results of the emittance growth for the largest LHeC circumference studied, 1/3 of LHC, can be found in Fig. 21.

The recent tracking studies demonstrated that the electron beam quality can be preserved until the IP in order to meet a normalised transverse emittance of

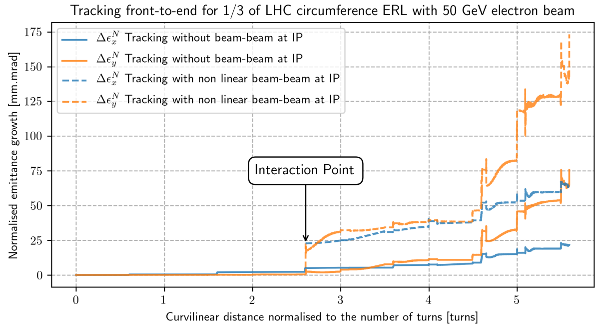

Fig. 21 Emittance growth along the curvilinear coordinate for the largest ERL design, corresponding to 1/3 of the LHC circumference.

30 mm mrad at the interaction point. Then, it is followed by a very strong non linear beam-beam interaction and finally decelerated over 3 turns to be dumped at 500 MeV. The tracking results of all the ERL circumferences studied, also including the synchrotron radiation and the beam-beam disruption, give an excellent transmissions of close to 100%, see Tab 6. The energy recovery efficiency is mainly constrained by the synchrotron light losses in the arcs that need to be compensated by extra RF cavities. It can be noted that the ERL designs, that consider smaller machine circumferences require a smaller horizontal injection emittance that will potentially not allow enough margin for further studies including magnet field errors and misalignment.

ERL size	1/3 C_{LHC}	1/4 C_{LHC}	1/5 C_{LHC}
$\gamma\varepsilon_x^{\mathrm{inj}}$ [µm rad]	25.4	22.7	15.1
$\Delta p/p$ at IP	0.021 %	0.029 %	0.041 %
transmission	99.93 %	98.89 %	98.40 %
energy recovery	97.9 %	96.7 %	95.4 %

Table 6 Results of the tracking simulations including beam-beam effect and synchrotron radiation for different ERL designs.

5 Summary

A detailed design has been presented for the introduction of a programme of high energy electron-hadron scattering in a future phase of running of the CERN Large Hadron Collider. The design is based on collisions at interaction point IP2, utilising one of the LHC hadron beams and assumes concurrent running with hadron-hadron collider experiments.

The electron beam is produced using two superconducting linear accelerators of length around 900 m each, arranged in a racetrack configuration with three separate return arcs, allowing acceleration in three turns to reach an energy of 50 GeV before bringing the beams into collision with the LHC hadrons. A key feature of the electron accelerator design is energy recovery, for which plans for a protoype (PERLE) are well-advanced. This allows electron currents of 20 mA to be foreseen, leading to instantaneous luminosities of order 10^{34} cm^{-2}s^{-1}.

The resulting LHeC experiment offers standalone sensitivity to a broad and original programme of physics at the energy frontier and also complements the existing LHC hadron-hadron experiments and their upgrades. Highlights of the high luminosity LHeC ep programme picked out in this document include probing the Higgs boson with competitive sensitivity to its WW and other couplings, studies of single top quark production with correspondingly high precision on the Wtb vertex and competitive sensitivity to physics beyond the standard model across a range of processes that benefit from initial state leptons. In heavy ion (eA) mode. In terms of hadron structure, the LHeC allows the extraction of parton densities with unprecedented precision, extending onto a new kinematic region at low Bjorken-x where new dynamics are expected. In eA mode, the LHeC offers unique sensitivity to nuclear parton densities and exploits their enhanced sensitivity to low x effects over those of the proton, as well as complementing the relativistic heavy ion collision programme at the LHC and RHIC by providing cold-matter baselines for the understanding of quark-gluon plasma effects and contributing to a range of topics with hard probes as well as soft physics and ultra-peripheral collisions.

The ambitious physics programme is matched by a hermetic, compact, high performance LHeC detector design based around a strong (3 T) central solenoid for the precision measurement of high transverse momentum charged particles. Inner detectors based on depleted MAPS silicon sensors will provide tracking and vertexing at the highest possible precision with a modest material budget. The pivotal importance of scattered electron detection and measurement in a DIS experiment is matched through electromagnetic calorimeter designs including an option based on cold liquid argon with lead absorbers, building on technologies used successfully in previous experiments. The need for a high quality hadron response, from high transverse momentum jets to the inclusive measurement of the hadronic final state for kinematic reconstruction, is met using a steel / scintillating tile solution. The importance of forward and very forward (and backward) instrumentation is recognised by implementing central detector components throughout the range $|\eta| < 5$ and by building beamline instrumentation in the outging hadron and electron directions into the interaction region design from the outset.

The addition of ep and eA capabilities to the CERN accelerator infrastructure, in combination with ongoing pp and AA programmes, deepens the sensitivity to new physics in the existing programme whilst introducing new possibilities particular to the presence of initial state leptons. Investigations are ongoing into the possibility of combining the LHeC plans with a future phase of AA collisions at IP2, amounting to a new multi-purpose detector capable of running in all beam modes. Whether part of a multi-purpose apparatus or operating in standalone mode, the LHeC offers new perspectives on an energy frontier physics landscape which may look rather different in the 2030s from that of today.

Acknowledgements This paper relies on a decade of work and collaboration with the hundreds of authors of the 2012 and 2020 LHeC design papers.

NA and EGF have received financial support from Xunta de Galicia (Centro singular de investigación de Galicia accreditation 2019-2022), by European Union ERDF, and by the "María de Maeztu" Units of Excellence program MDM2016-0692 and the Spanish Research State Agency under project FPA2017-83814-P. NA and JGM are supported by the European research Council under project ERC-2018-ADG-835105 YoctoLHC. NA is also supported by MSCA RISE 823947 "Heavy ion collisions: collectivity and precision in saturation physics" (HIEIC), and JGM by Fundaçao para a Ciência e a Tecnologia (Portugal) under project CERN/FISPAR/0024-/2019, and he gratefully acknowledges the hospitality of the CERN theory group. NA, EGF and JGM have received funding from the European Union's Horizon 2020 research and innovation programme under grant agreement No. 824093.

MK, BM and XR are grateful for the support from the South African Department of Science and Innovation, and the National Research Foundation.

Very fruitful discussions are acknowledged which some of us had with John Jowett.

References

1. J. L. Abelleira Fernandez *et al.* [LHeC Study Group], J. Phys. G **39** (2012), 075001 doi:10.1088/0954-3899/39/7/075001 [arXiv:1206.2913 [physics.acc-ph]].
2. O. Brüning *et al.* [LHeC and PERLE], J. Phys. G **46** (2019) no.12, 123001 doi:10.1088/1361-6471/ab4698
3. P. Agostini *et al.* [LHeC and FCC-he Study Group], [arXiv:2007.14491 [hep-ex]].
4. D. Adamová, G. Aglieri Rinella, M. Agnello, Z. Ahammed, D. Aleksandrov, A. Alici, A. Alkin, T. Alt, I. Altsybeev and D. Andreou, *et al.* [arXiv:1902.01211 [physics.ins-det]].
5. O. Brüning and M. Klein, "Electrons for the LHC – on the update of the LHeC CDR on Physics, Accelerator and Detector", in [ECFA Newsletter 5, ed. J.de Hondt, CERN 2020, unpublished.]
6. S. Dutta, A. Goyal, M. Kumar and B. Mellado, Eur. Phys. J. C **75** (2015) no.12, 577 doi:10.1140/epjc/s10052-015-3776-z [arXiv:1307.1688 [hep-ph]].

7. M. Gao and J. Gao, [arXiv:2103.15846 [hep-ph]].
8. H. Sun, PoS **DIS2018** (2018), 167 doi:10.22323/1.316.0167
9. E. Alvarez, L. Da Rold, M. Estevez and J. F. Kamenik, Phys. Rev. D **97** (2018) no.3, 033002 doi:10.1103/PhysRevD.97.033002 [arXiv:1709.07887 [hep-ph]].
10. A. O. Bouzas and F. Larios, Phys. Rev. D **88** (2013) no.9, 094007 doi:10.1103/PhysRevD.88.094007 [arXiv:1308.5634 [hep-ph]].
11. I. Turk Cakir, A. Yilmaz, H. Denizli, A. Senol, H. Karadeniz and O. Cakir, Adv. High Energy Phys. **2017** (2017), 1572053 doi:10.1155/2017/1572053 [arXiv:1705.05419 [hep-ph]].
12. S. Behera, R. Islam, M. Kumar, P. Poulose and R. Rahaman, Phys. Rev. D **100** (2019) no.1, 015006 doi:10.1103/PhysRevD.100.015006 [arXiv:1811.04681 [hep-ph]].
13. S. Atag and B. Sahin, Phys. Rev. D **73**, 074001 (2006).
14. T. Han and B. Mellado, Phys. Rev. D **82** (2010), 016009 doi:10.1103/PhysRevD.82.016009 [arXiv:0909.2460 [hep-ph]].
15. S. S. Biswal, R. M. Godbole, B. Mellado and S. Raychaudhuri, Phys. Rev. Lett. **109** (2012), 261801 doi:10.1103/PhysRevLett.109.261801 [arXiv:1203.6285 [hep-ph]].
16. M. Kumar, X. Ruan, R. Islam, A. S. Cornell, M. Klein, U. Klein and B. Mellado, Phys. Lett. B **764** (2017), 247-253 doi:10.1016/j.physletb.2016.11.039 [arXiv:1509.04016 [hep-ph]].
17. B. Coleppa, M. Kumar, S. Kumar and B. Mellado, Phys. Lett. B **770** (2017), 335-341 doi:10.1016/j.physletb.2017.05.006 [arXiv:1702.03426 [hep-ph]].
18. S. Antusch, O. Fischer and A. Hammad, JHEP **03** (2020), 110 doi:10.1007/JHEP03(2020)110 [arXiv:1908.02852 [hep-ph]].
19. L. Delle Rose, O. Fischer and A. Hammad, Int. J. Mod. Phys. A **34** (2019) no.23, 1950127 doi:10.1142/S0217751X19501276 [arXiv:1809.04321 [hep-ph]].
20. D. Curtin, K. Deshpande, O. Fischer and J. Zurita, JHEP **07** (2018), 024 doi:10.1007/JHEP07(2018)024 [arXiv:1712.07135 [hep-ph]].
21. D. Curtin, K. Deshpande, O. Fischer and J. Zurita, Phys. Rev. D **99** (2019) no.5, 055011 doi:10.1103/PhysRevD.99.055011 [arXiv:1812.01568 [hep-ph]].
22. S. Antusch, A. Hammad and A. Rashed, JHEP **03** (2021), 230 doi:10.1007/JHEP03(2021)230 [arXiv:2010.08907 [hep-ph]].
23. A. Das, S. Mandal and T. Modak, Phys. Rev. D **102** (2020) no.3, 033001 doi:10.1103/PhysRevD.102.033001 [arXiv:2005.02267 [hep-ph]].
24. X. H. Yang and Z. J. Yang, [arXiv:2103.11412 [hep-ph]].
25. G. Azuelos, O. Fischer and S. Jana, [arXiv:2012.11514 [hep-ph]].
26. R. Padhan, S. Mandal, M. Mitra and N. Sinha, Phys. Rev. D **101** (2020) no.7, 075037 doi:10.1103/PhysRevD.101.075037 [arXiv:1912.07236 [hep-ph]].
27. G. Cottin, O. Fischer, S. Mandal, M. Mitra and R. Padhan, [arXiv:2104.13578 [hep-ph]].
28. G. D. Kribs, D. McKeen and N. Raj, Phys. Rev. Lett. **126** (2021) no.1, 011801 doi:10.1103/PhysRevLett.126.011801 [arXiv:2007.15655 [hep-ph]].
29. M. D'Onofrio, O. Fischer and Z. S. Wang, Phys. Rev. D **101** (2020) no.1, 015020 doi:10.1103/PhysRevD.101.015020 [arXiv:1909.02312 [hep-ph]].
30. R. Preghenella [ALICE], "Perspectives for particle identification in ALICE using silicon-based timing detectors," PoS **LHCP2020** (2021), 078 doi:10.22323/1.382.0078 [arXiv:2010.06913 [physics.ins-det]].
31. R. K. Ellis, B. Heinemann, J. de Blas, M. Cepeda, C. Grojean, F. Maltoni, A. Nisati, E. Petit, R. Rattazzi and W. Verkerke, *et al.* [arXiv:1910.11775 [hep-ex]].
32. Z. Citron, A. Dainese, J. F. Grosse-Oetringhaus, J. M. Jowett, Y. J. Lee, U. A. Wiedemann, M. Winn, A. Andronic, F. Bellini and E. Bruna, *et al.* CERN Yellow Rep. Monogr. **7** (2019), 1159-1410 doi:10.23731/CYRM-2019-007.1159 [arXiv:1812.06772 [hep-ph]].
33. L. Apolinário, J. G. Milhano, G. P. Salam and C. A. Salgado, Phys. Rev. Lett. **120** (2018) no.23, 232301 doi:10.1103/PhysRevLett.120.232301 [arXiv:1711.03105 [hep-ph]].
34. A. Huss, A. Kurkela, A. Mazeliauskas, R. Paatelainen, W. van der Schee and U. A. Wiedemann, Phys. Rev. Lett. **126** (2021) no.19, 192301 doi:10.1103/PhysRevLett.126.192301 [arXiv:2007.13754 [hep-ph]].
35. K. J. Eskola, P. Paakkinen, H. Paukkunen and C. A. Salgado, Eur. Phys. J. C **77** (2017) no.3, 163 doi:10.1140/epjc/s10052-017-4725-9 [arXiv:1612.05741 [hep-ph]].
36. K. J. Eskola, P. Paakkinen and H. Paukkunen, Eur. Phys. J. C **79** (2019) no.6, 511 doi:10.1140/epjc/s10052-019-6982-2 [arXiv:1903.09832 [hep-ph]].
37. K. J. Eskola, I. Helenius, P. Paakkinen and H. Paukkunen, JHEP **05** (2020), 037 doi:10.1007/JHEP05(2020)037 [arXiv:1906.02512 [hep-ph]].
38. [ALICE], ALICE-PUBLIC-2018-013; CERN-LHCC-2019-018 ; LHCC-I-034.
39. [ALICE], CERN-LHCC-2020-009.
40. J. L. Nagle and W. A. Zajc, Ann. Rev. Nucl. Part. Sci. **68** (2018), 211-235 doi:10.1146/annurev-nucl-101916-123209 [arXiv:1801.03477 [nucl-ex]].
41. J. Collins, Camb. Monogr. Part. Phys. Nucl. Phys. Cosmol. **32** (2011), 1-624
42. U. Heinz and R. Snellings, Ann. Rev. Nucl. Part. Sci. **63** (2013), 123-151 doi:10.1146/annurev-nucl-102212-170540 [arXiv:1301.2826 [nucl-th]].
43. A. Andronic, F. Arleo, R. Arnaldi, A. Beraudo, E. Bruna, D. Caffarri, Z. C. del Valle, J. G. Contreras, T. Dahms and A. Dainese, *et al.* Eur. Phys. J. C **76** (2016) no.3, 107 doi:10.1140/epjc/s10052-015-3819-5 [arXiv:1506.03981 [nucl-ex]].
44. F. Bordry, M. Benedikt, O. Brüning, J. Jowett, L. Rossi, D. Schulte, S. Stapnes and F. Zimmermann, [arXiv:1810.13022 [physics.acc-ph]].
45. H. Abramowicz *et al.* [H1 and ZEUS], Eur. Phys. J. C **75** (2015) no.12, 580 doi:10.1140/epjc/s10052-015-3710-4 [arXiv:1506.06042 [hep-ex]].
46. Y. Mehtar-Tani, J. G. Milhano and K. Tywoniuk, Int. J. Mod. Phys. A **28** (2013), 1340013 doi:10.1142/S0217751X13400137 [arXiv:1302.2579 [hep-ph]].
47. H. T. Li and I. Vitev, [arXiv:2010.05912 [hep-ph]].
48. C. Andres, N. Armesto, H. Niemi, R. Paatelainen and C. A. Salgado, Phys. Lett. B **803** (2020), 135318 doi:10.1016/j.physletb.2020.135318 [arXiv:1902.03231 [hep-ph]].

49. S. Klein, D. Tapia Takaki, J. Adam, C. Aidala, A. Angerami, B. Audurier, C. Bertulani, C. Bierlich, B. Blok and J. D. Brandenburg, *et al.* [arXiv:2009.03838 [hep-ph]].
50. G. Aad *et al.* ATLAS, [arXiv:2101.10771 [nucl-ex]].
51. G. Aad *et al.*, ATLAS, Phys. Rev. Lett. **123** (2019) no.5, 052001 doi:10.1103/PhysRevLett.123.052001 [arXiv:1904.03536 [hep-ex]].
52. V. Bertone, M. Cacciari, S. Frixione and G. Stagnitto, JHEP **03** (2020), 135 doi:10.1007/JHEP03(2020)135 [arXiv:1911.12040 [hep-ph]].
53. M. Frank, F. Gaede, M. Petric, A. Sailer, AIDASoft/DD4hep, https://dd4hep.web.cern.ch/dd4hep/, doi:10.5281/zenodo.592244
54. M. Mager, https://pos.sissa.it/373/040/pdf The 28th International Workshop on Vertex Detectors (VERTEX), 13–18 October 2019 Lafodia Sea Resort, Lopud Island, Croatia doi:10.22323/1.373.0040
55. G. A. Rinella *et al.* [ALICE ITS project and Nuclear Physics Group, STFC Daresbury Laboratory, Daresbury, United Kingdom], "First demonstration of in-beam performance of bent Monolithic Active Pixel Sensors," [arXiv:2105.13000 [physics.ins-det]].
56. G. Bianchi, "tkLayout: a design tool for innovative silicon tracking detectors," doi:10.1088/1748-0221/9/03/C03054
57. LHeC Study group, "The Large Hadron-Electron Collider at the HL-LHC," CERN, Geneva, Tech. Rep., Jan. 2020, Submitted to J.Phys. arXiv: 2007.14491. [Online]. Available: https : / / cds . cern . ch / record/2706220.
58. F. Marhauser, "Recent results on a multi-cell 802 Mhz bulk Nb cavity." Presented at FCC week 2018, https://indico.cern.ch/event/656491.
59. PERLE Collaboration, M. Klein, A. Stocchi et al., "PERLE: A High Power Energy Recovery Facility for Europe," A Contribution to the Update of the European Strategy on Particle Physics, CERN-ACC-NOTE-2018-0086, Dec 2018.
60. D. Pellegrini, A. Latina, D. Schulte, S.A. Bogacz, "Beam-dynamics Driven Design of the LHeC Energy Recovery Linac", PRST-AB, 18, 121004 (2015)
61. I. Bejar Alonso et al., "High-Luminosity Large Hadron Collider (HL-LHC)", technical design report, CERN-2020-010
62. S. Russenschuck, "Field computation for accelerator magnets: analytical and numerical methods for electromagnetic design and optimization', Wiley, Weinheim, 2010.
63. K. D. J. André, "Beam Dynamics and Lattice Design for the Large Hadron electron Collider", PhD thesis, in preparation.
64. L. J. Nevay et al., "BDSIM: An Accelerator Tracking Code with Particle-Matter Interactions", Computer Physics Communications 252 107200 (2020).
65. LHeC Study group, "The Large Hadron Electron Collider at the HL-LHC", CERN ACC-Note 2020-0002, CERN Geneva 2020.
66. D. Pellegrini, "Beam dynamics studies in recirculating machines", Ph.D. dissertation, école polytechnique fédérale de Lausanne, 2016.
67. I. Perić, doi:10.1109/NSSMIC.2007.4437188
68. A. Blondel, A. Bravar, M. Pohl, S. Bachmann, N. Berger, M. Kiehn, A. Schoning, D. Wiedner, B. Windelband and P. Eckert, *et al.* "Research Proposal for an Experiment to Search for the Decay $\mu \to eee$," [arXiv:1301.6113 [physics.ins-det]].
69. A. Gabrielli, "Commissioning of ROD boards for the entire ATLAS Pixel Detector," doi:10.1088/1748-0221/13/09/T09009
70. T. Ackernley *et al.* "Mighty Tracker: Design studies for the downstream silicon tracker in Upgrade Ib and II", LHCb-INT-2019-007
71. L. Linnssen *et al.* "Physics and Detectors at CLIC: CLIC Conceptual Design Report," arXiv:1202.5940
72. H1 Collaboration, A. Babaev, *Performance of the H1 liquid argon calorimeter*, (1994) . 5th International Conference on Calorimetry in High-energy Physics, Published in Calorimetry in high energy physics, River Edge, N.J., World Scientific, 1995. 524p.
73. H1 Collaboration, I. Abt et al., *The H1 detector at HERA*, http://dx.doi.org/10.1016/S0168-9002(96)00893-5Nucl.Instrum.Meth. **A386** (1997) 310–347.
74. M. Fleischer, M. Keller, K. Meier, O. Nix, G. Schmidt, et al., *Performance and upgrade of H1 calorimeters: LAr calorimeter, SpaCal and VLQ*, (1997) . DESY-98-005.
75. C. Issever, *The calibration of the H1 liquid argon calorimeter*, (2000) . presented at 9th Conference on Calorimetry in High Energy Physics (CALOR 2000), CALORIMETRY IN HIGH ENERGY PHYSICS: Proceedings. Edited by B. Aubert, J. Colas, P. Nedelec, L. Poggioli. Frascati, Italy, Istituto Naz. Fis. Nucl., 2001. 843p. (Frascati Physics Series, Vol. 21), pages 603-608.
76. H1 collaboration, C. Schwanenberger, *The Jet calibration in the H1 liquid argon calorimeter*, http://arxiv.org/abs/physics/0209026`arXiv:physics/0209026 [physics]`.
77. J. Seehafer, *Simulation of hadronic showers in the H1 liquid argon calorimeter with the simulation programs GHEISHA and CALOR*, (2005) .
78. C. Kiesling, A. Dubak, and B. Olivier, *The liquid argon jet trigger of the H1 experiment at HERA*, http://dx.doi.org/10.1016/j.nima.2010.03.054Nucl.Instrum.Meth. **A623** (2010) 513–515.
79. ATLAS Electromagnetic Barrel Liquid Argon Calorimeter Group, B. Aubert et al., *Construction, assembly and tests of the ATLAS electromagnetic barrel calorimeter*, http://dx.doi.org/10.1016/j.nima.2005.11.212Nucl.Instrum.Meth. **A558** (2006) 388–418.
80. ATLAS collaboration, *ATLAS liquid argon calorimeter: Technical design report*, CERN-LHCC-96-41, (1996).
81. S. Morgenstern et al, *ATLAS LAr calorimeter performance in LHC Run-2*, ATL-LARG-PROC-2018-004, Nucl. Instrum. Meth. **A936** (2019) 86–89, doi:10.1016/j.nima.2018.11.027
82. GEANT4 Collaboration, S. Agostinelli et al., *GEANT4: A Simulation toolkit*, http://dx.doi.org/10.1016/S0168-9002(03)01368-8Nucl.Instrum.Meth. **A506** (2003) 250–303.
83. V. Boudry, Vincent, CALICE Coallaboration, *Implementation of large imaging calorimeters*, doi:10.22323/1.390.0823
84. H.G. Cabrera, CALICE Coallaboration, *SDHCAL technological prototype test beam results*, Talk presented at the International Workshop on Future Linear Colliders (LCWS2021), 15-18 March 2021. C21-03-15.1, arXiv:2105.06585 [physics.ins-det]
85. P. Yock, Phys. Essays **33** (2020) no.2, 149-158 doi:10.4006/0836-1398-33.2.149
86. K. Kawagoe and L.K. Emberger, CALICE Coallaboration, *Toward Realistic Implementations of Large Imaging Calorimeters*, PoS 2019 LeptonPhoton2019), doi:10.22323/1.367.0151,
87. ATLAS Collaboration, *Technical Design Report for the Phase-II Upgrade of the ATLAS Muon Spectrometer* CERN-LHCC-2017-017, ATLAS-TDR-026 https://cds.cern.ch/record/2285580https://cds.cern.ch/record/2285580

88. CMS Collaboration, *The Phase-2 Upgrade of the CMS Muon Detectors* CERN-LHCC-2017-012 ; CMS-TDR-016 https://cds.cern.ch/record/2283189https://cds.cern.ch/record/2283189